5

Mapping Soil Salinization of Agricultural Coastal Areas in Southeast Spain

Ignacio Melendez-Pastor, Encarni I. Hernández,
Jose Navarro-Pedreño and Ignacio Gómez
Department of Agrochemistry and Environment,
University Miguel Hernández of Elche
Spain

1. Introduction

Soil salt content is a key factor that determines soil chemical quality together with soil reaction, charge properties and nutrient reserves (Lal et al., 1999). An adequate salt supply is essential for an optimum development of photosynthetic mechanism and other biochemical processes in plants (Sitte et al., 1994). Soil salt content constitutes an environmental problem when salt accumulation generates drastic changes in soil physical and chemical properties, adversely affecting soil productivity and plant growth (Richards, 1954; Qadir et al., 2000).

Salinization affects about 30% of the irrigated land of the world, decreasing this area approximately 1-2% per year due to salt-affected land surfaces (FAO, 2002). In Europe, about 1-3 million hectares of the land are affected by salinization (European Commission, 2003), and most of these areas are situated in the Mediterranean basin. In Spain, about 18% of the 3.5 million hectares of irrigated land are severely affected or at serious risk of soil salinization (European Commission, 2002). Soil salinization is a frequent problem in arid and semiarid regions like Southeast Spain (Hernández Bastida et al., 2004). In these areas, agriculture with a great water requirement combined with high water tables and an adverse climate (increased occurrence of extreme drought events) have forced irrigation with poor quality water, causing processes of soil degradation and salinization, limiting crop growth and the production capacity (Pérez-Sirvent et al., 2003; Acosta et al., 2011).

Evaluating the spatial variability of basic soil properties in saline soils, and mapping spatial distribution patterns of these soil properties helps to make effective site-specific management decisions (Ardahanlioglu et al., 2003). Accordingly, remote sensing techniques and geographic information systems (GIS) have introduced a new era for soil resources assessment and monitoring in terms of information quality (Mermut and Eswaran, 2001). *A priori* knowledge of spectral characteristics of remotely sensed materials is fundamental to any valuable quantitative analysis (Ben-Dor et al., 1997). The variety of absorption processes occurring in the soil and their wavelength dependence allow us to derive information about the chemistry of the minerals composing it from the reflected or emitted light (Clark, 1999). Reflectance spectra of soils are attributed to numerous soil properties. There are no narrow absorption bands linked to soil salinity status, since it is

determined by soil properties such as pH, electrical conductivity, salt content and exchangeable sodium percentage (Csillag et al., 1993; Farifteh et al., 2008). In this sense, soil reflectance is derived from the particular spectral behaviour of the heterogeneous combination of minerals, organic matter and soil water (Ben-Dor and Banin, 1994). Salt-affected soils cations (Na^+, Mg^{2+}, K^+, and Ca^{2+}) and anions (Cl^-, SO_4^{2-}, CO_3^{2-} and HCO_3^-) can be detected by optical spectrometers since salt minerals have diagnostic spectral features occurring in the visible and near infrared (VNIR) and short-wave infrared (SWIR) spectral regions (Farifteh et al., 2008). Saline soils usually have evaporate minerals, which spectral features that can be explained by vibrational absorption due to water molecules chemically bound as part of the crystal structure (Howari et al., 2000). In this sense, the spectral differences of evaporates of single salt compounds are determinant of the type and mineralogy of the soils (Howari et al., 2000).

Remote sensing has been extensively employed in soil salinity studies. Data from aerial photography, videography, and optical, thermal, microwave or geophysical sensors has been used in soil salinity mapping (Metternich and Zinck, 2003). Perhaps, the most widely used remote sensing data in recent decades have been provided by multispectral (Landsat, SPOT, IRS, ASTER) or hyperspectral (DAIS, HyMap, AVIRIS, Hyperion) sensors in the spectral range approximately between 400 and 2500 nm. Researchers have frequently employed remote sensing data to map soil salinity with multispectral (Metternich and Zinck, 1997; Dwivedi et al., 2001; Melendez-Pastor et al., 2010a) and hyperspectral images (Dehaan and Taylor, 2002, 2003; Schmid et al., 2009, Ghrefat and Goodell, 2011). Pioneering studies in the 1970s employed air-borne and satellite-borne multispectral scanners to detect soil salinity, indicating the better capability of infrared bands over visible bands to locate saline soils and the low contribution of thermal bands to improve the delineation of saline areas (Richardson et al., 1976; Dalsted et al., 1979). Nowadays, imaging spectroscopy techniques are employed for the automatic detection of soil salinization with airborne or satellite sensor (Dehaan and Taylor, 2002, 2003; Dutkiewicz et al., 2009; Schmid et al., 2009; Weng et al., 2009; Melendez-Pastor et al., 2010a; Ghrefat and Goodell, 2011). Imaging spectroscopy deals with the mapping of ground materials by detecting and analysing reflectance/absorbance features in hyperspectral (or multispectral) images (Clark, 1999). Imaging spectroscopy adds a new dimension of remote sensing by expanding point spectrometry into a spatial domain and under field conditions, which is a very good approach for the study of soil properties (Ben-Dor et al., 2009).

The aim of this chapter is the application of remote sensing for the study of soil salinity of an agricultural area in southeast coast of the Iberian Peninsula. Different digital image processing techniques were applied to satellite multispectral images (Landsat TM). 'Conventional' hard classification techniques were combined with spectral mixture analysis and soil properties to achieve a better understanding of the soil salinization process in the study area.

Multispectral satellite images such as those obtained by the Landsat program provide low or free cost worldwide coverage for four decades. Moreover, salinization problems are concentrated in arid and semi-arid regions, often in developing countries with few economic resources. Although there are more advanced sensors that can provide a more precise quantification of the extent of soil salinity (e.g. hyperspectral), their high cost difficult its

extensive use. Therefore, it is necessary to continue investigating the application of multispectral image repositories as a tool to assist in the monitoring and management of saline soils.

2. Material and methods

This study will evaluate the applicability of various remote sensing techniques for studying salinization processes in an agricultural coastal area. One of the greatest difficulties in the application of remote sensing techniques to the study area is the fragmentation of the territory by the existence of small plots and buildings that create a dispersed mixture of spectral signals to the scale of a moderate spatial resolution multispectral remote sensing image as those acquired by the Landsat Thematic Mapper sensor. This difficulty motivates the need to evaluate various techniques and methodological approaches to carry out this study as necessary to help monitoring the processes of salinization.

Representative soils of the area were sampled and their properties were characterized at the laboratory by standard methods. Predominant land cover classes at the soil sampling plots and at additional land cover validation points were identified. Land cover is a fundamental variable that impacts on and links many parts of the human and physical environments (Foody, 2002) with a great influence on soil properties (Caravaca et al., 2002; Majaliwa et al., 2010; Biro et al., 2011). Both kinds of information in a GIS database were included. In this sense, the effect of land cover on soil properties was statistically evaluated. Then, multispectral images were employed for a hard land cover mapping with a supervised approach using the k-nearest-neighbour classifier. Accuracy assessment methods highlighted the need to employ a mixed pixel focus to deal with the particularities of the study area. Spectral unmixing techniques allowed the identification of representative spectral endmembers and the obtainment of their corresponding fraction images. Finally, fraction endmembers were employed to characterize land cover classes and to predict soil properties with various statistical methods.

2.1 Description of the study area

The study area is located in a coastal zone of Southeast Spain, in the province of Alicante. It is located around 38.14°N and 0.73ºW, at the south of the cities of Elche and Alicante. The study area (Figure 1) comprises alluvial plains resulting from the accumulation of sediments from the Segura and Vinalopó rivers. During most of the Holocene (~10,000 years ago to present) the study area was a large lagoon (Blázquez, 2003). In the last centuries, the ancient lagoon was transformed into an irrigated agricultural land draining the wetland. Nowadays, this area is a mixture of small-size cities, coastal urban areas, scattered residential houses, irrigated crops and isolated and scattered wetlands. The perimeter of the study area was delimited according to natural or man-made features in order to enclose a large coastal plain area primarily occupied by irrigated agricultural activities. The study area lies in the north with the natural parks of *El Hondo* and the *Salinas de Santa Pola*. Both natural areas are wetlands included in the RAMSAR list of wetlands of international importance. The east and south boundaries are the *Sierra del Molar* and the *Segura River* respectively. Urban areas and sclerophyllous vegetation mainly occupy the Sierra del Molar, while the Segura River is the most important watercourse in southeast of Iberian Peninsula providing water for irrigation agriculture and to fill the reservoirs that currently comprise

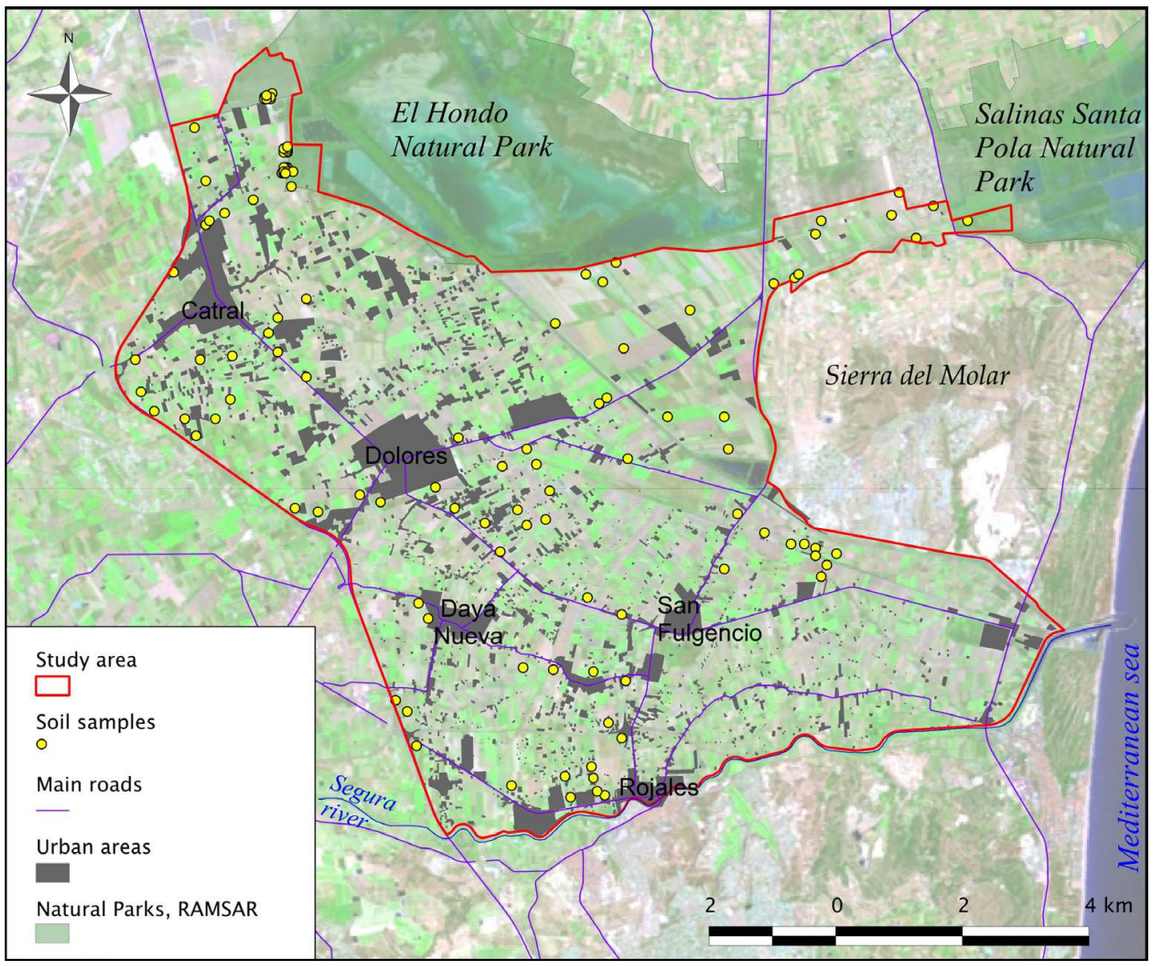

Fig. 1. Study area with the Landsat scene (false-colour composite RGB:742) and superimposed cartographic information (soil samples, urban areas, natural parks and roads).

the wetland of *El Hondo*. The western boundary of the study area is a motorway that cuts north to south the floodplain.

This coastal region has a semiarid Mediterranean climate, with a mean annual rainfall of less than 300 mm and a mean annual temperature of 17 ºC and defined by the Köppen climate classification system as *Bsk* class (dry climate with a dry season in summer and a mean annual temperature about 18 ºC). The climate is arid or semiarid according to the aridity index of Martonne (De Martonne, 1926) and the aridity index of UNEP (1997) respectively. Figure 2 shows the daily climatic diagram of mean temperature, precipitation and evapotranspiration (by the Penman-Monteith method) for the hydrological year 2010-2011 (from October to September) at Catral meteorological station. Mean daily temperature (blue line) varies from approximately 9ºC in winter to more than 25ºC in summer. Rain events (red bars) mainly occurred from December 2010 to May 2011 with total accumulated precipitation of 182 mm. This very scarce precipitation joint with an accumulated evapotranspiration of 1115 mm implied that the hydrological year was very dry.

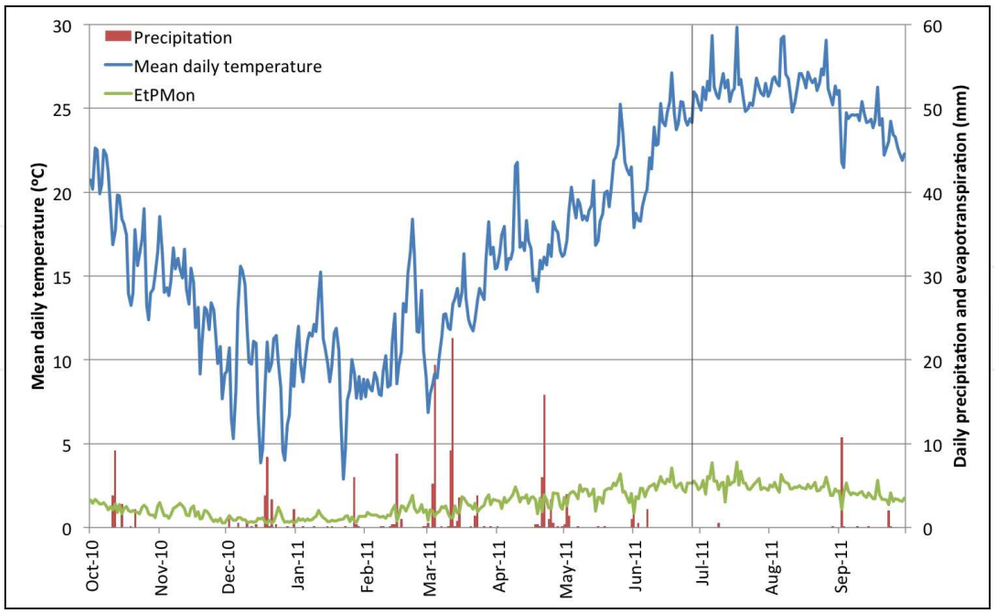

Fig. 2. Daily values of precipitation, mean temperature and evapotranspiration for the hydrological year 2010-11 at Catral station. Source data from the Spanish Ministry of Environment and Rural and Marine Affairs (MARM).

Predominant soil classes are Entisols according to the Soil Taxonomy (Soil Survey Staff, 2006) but affected by agriculture practices along years. They are characterized by a massive presence of carbonates and soluble salt content. In the studied area, irrigation is essential to support agriculture. The water deficit during several months requires irrigation while low quality water is used in the poorly drained soils of these coastal plains, being soil salinization an environmental problem. Thus, the study area soils are subjected to severe risk of physical, chemical and biological degradation (De Paz et al., 2006) that endanger agriculture sustainability.

2.2 Field survey

Field survey was done in the late spring and summer months of the hydrological year 2010-2011 to collect soil samples and identify land cover classes. An extensive soil sampling was done, and 116 samples were collected and geographically referenced. Samples were obtained from the upper 5 cm as solar radiation in VNIR spectral range has limited penetration capabilities. Soil samples were dried at room temperature and a 2 mm sieve was used to separate the fine fraction to be analysed. Analysed soil characteristics included in the study were electrical conductivity (EC) (1:5 w/v water extraction), pH and organic carbon (OC) by wet chemical oxidation (Walkley and Black, 1934) with potassium dichromate oxidation (Nelson and Sommers, 1982).

A land cover validation campaign was also conducted along with the soil survey in order to allow accuracy assessment of generated land cover maps. Land cover validation points were randomly generated in a GIS and a database with the land cover category generated. A total of 205 land cover validation points were identified, combining field observation and recent aerial orto-photography (0.5 m of spatial resolution). Land cover classes identified in the

study area were: water bodies, seasonal or permanent crops, saltmarshes and misused agricultural field that tends to be saltmarshes, palm groves, marshes with almost permanent inundation, and anthropic areas (Table 1).

Land cover	ID	Features
Water	1	Wetlands water tables and irrigation ponds
Arable land	2	Herbaceous (e.g. alfalfa, barley) and horticultural (e.g. melon, broccoli) crops
Permanent crops	3	Fruit trees (e.g. orange, lemon, pomegranate)
Fallow/abandoned	4	Fallow or recently abandoned agricultural land.
Saltmarsh	5	Halophyte vegetation (e.g. *Salicornia sp*., *Suaeda sp*., *Limonium sp*., *Halocnemum sp*.)
Palm groves	6	Palm trees plantations and nurseries, mainly from *Phoenix dactilifera*
Marsh	7	*Phragmites australis* dominated wetland vegetation
Man-made/urban	8	Urban areas, roads, farms or industrial areas

Table 1. Descriptions of land cover classes identified in the study area.

Land cover categories at soil sampling points were also identified and included along with soil properties in a GIS database for the land cover classification training stage and for further spatial analyses. Note that land cover (i.e. biophysical materials found on the land) and land use (i.e. how the land is being used by human beings) (Jensen, 2007) are different terms but often used together or interchangeably. In this chapter, we adopt the term land cover because we are interested in knowing about the biophysical characteristics of the study area, but the knowledge of both land use and land cover are important for land planning and land management activities (Lillesand et al., 2003).

2.3 Satellite imagery preprocessing

Remote sensing data were acquired by the Thematic Mapper (TM) sensor on-board the Landsat 5 satellite. Meteorological conditions and the satellite pass over the study area conditioned the date of image acquisition. A scene acquired on 28th June 2011 (path 199 row 33) was employed for analyses. A vertical black line on Figure 2 indicates the time of acquisition of the scene. No rain events happened 16 days prior to the scene acquisition date. Typically summer meteorological conditions without cloud coverage and high temperature were registered on the date of image acquisition, and thus the image quality was optimal.

Satellite image preprocessing included geometric and atmospheric corrections with the aim to ensure the spatial comparability with other data sources and to obtain at-ground reflectance pixel spectra, respectively. Various georeferenced data types were used for the geometric correction: aerial orthophotos (0.5 m of pixel resolution) and digital cartography (scale = 1:10000). The Landsat 5 TM scene was geometrically corrected using Ground Control Points (GCP) identified on the orthophotos and cartographic maps. A quadratic mapping function of polynomial fit and the nearest neighbour resampling method were

used for the correction. The nearest neighbour resampling method was selected because it ensures that the original (raw) pixel values are retained in the resulting output image, which is an important requirement in any change detection analysis (Mather 2004). The maximum allowable root mean square error (RMSE) of the geometric correction was less than half a pixel, a reference value frequently cited (Townsend and Walsh 2001; Jensen, 2005).

Atmospheric correction involves the estimation of the atmospheric optical characteristics at the time of image acquisition before applying the correction to the data (Kaufman, 1989). This type of correction is a pre-requisite in many remote sensing applications such as in classification and change detection procedures (Song et al., 2001). Radiometric calibration was applied prior to the atmospheric correction. The conversion of raw digital numbers (DN_{raw}) of Landsat level 1 (L1) image products to at-satellite radiance values (L_{sat}) required the application of current re-scaling values (Chander et al., 2010) by applying the following expression (Chander and Markham, 2003; Chander et al., 2010):

$$L_{\text{sat}} = \left(\frac{L_{\text{MAX}\,\lambda} - L_{\text{MIN}\,\lambda}}{255} \right) (\text{DN}) + L_{\text{MIN}\,\lambda} \tag{1}$$

Where L_{sat} is at-satellite radiance [W/(m² sr μm)]; $L_{MIN\,\lambda}$ is the spectral radiance that is scaled to Q_{calmin} [W/(m² sr μm)] (Q_{calmin} is the minimum quantized calibrated pixel value, i.e. DN=0, corresponding to $L_{MIN\,\lambda}$); $L_{MAX\,\lambda}$ is the spectral radiance that is scaled to Q_{calmax} [W/(m² sr μm)] (Q_{calmax} is the maximum quantized calibrated pixel value, i.e. DN=255, corresponding to $L_{MAX\,\lambda}$); and DN are digital numbers of the L1 image product. Surface reflectance values (ρ) were computed by using the image based COST method (Chavez Jr, 1996). Path radiance (L_p) values were computed by using the equation reported in Song et al. (2001) that assumes 1% surface reflectance for dark objects (Chavez Jr, 1989, 1996; Moran et al., 1992). The optical thickness for Rayleigh scattering (τ_r) was estimated according to the equation given in Kaufman (1989).

2.4 Land cover classification

Image classification procedures aim to automatically categorize all pixels in an image into land cover classes or themes (Lillesand et al., 2003). Thematic mapping from remotely sensed data can be defined as grouping together cases (pixels) by their relative spectral similarity (unsupervised component) with the aim of allocating cases based on their similarity to a set of predefined classes that have been characterized spectrally (supervised component) (Foody 2002). Multispectral images (like Landsat TM scenes) are frequently used to perform the classification based on spectral pattern recognition methods that exploits the pixel-by-pixel spectral information as the basis for automated classification (Lillesand et al., 2003). In this study, a supervised land cover classification of the Landsat TM image was performed with a *k*-nearest-neighbour clustering algorithm to obtain a discrete or 'hard' categorical land cover map for the study area. *K*-nearest-neighbour (KNN) classifier searches away from the pixel to be classified in all directions of the spectral space until it encounters *k* user-specified training pixels and then assigns the pixel to the class with the majority of pixels encountered (Jensen, 2005). KNN algorithm has been successfully applied for land cover classification with remote sensing data (Franco-Lopez et al., 2001; Haapanen et al., 2004; Blanzieri and Melgani, 2008). Land cover classes assigned to the soil plots were employed in the training stage of the

algorithm. Major urban areas were digitized with a GIS and masked-out of the supervised classification procedure since urban areas induce a great spectral confusion. Water areas training points were also included in the training dataset.

The land cover validation database was employed to evaluate the performance of the classification. Land cover map accuracy assessment was quantified with statistical methods such as the error matrix and the kappa statistic. The error matrix is a square array of numbers organized in rows and columns that express the number of sample units (i.e. pixels) assigned to a particular category relative to the actual category as indicated by the reference data (Congalton, 2004). Reference data are in the columns while the rows indicate the map categories to be assessed. This form of expressing accuracy as an error matrix is an effective way to evaluate both errors of inclusion (commission errors) and errors of exclusion (omission errors) present in the classification as well as the overall accuracy (Congalton et al., 1983). In addition to the error matrix, the Kappa coefficient developed by Cohen (1960) was employed to quantify the accuracy of the land cover map. Cohen's Kappa (or KHAT) is a measure of agreement for nominal scales based on the difference between the actual agreement of the classification (i.e., agreement between computer classification and reference data as indicated by the diagonal elements) and the chance agreement, which is indicated by the product of the row and column marginal (Congalton et al., 1993).

2.5 Spectral unmixing

A mixed pixel results when a sensor's Instantaneous Field of View (IFOV) includes more than one land cover type on the ground (Lillesand et al., 2003). The spectrum of a single pixel is a complex measurement that integrates the radiant flux from all the spatially unresolved materials in the IFOV, regardless of whether or not we know their identities (Adams and Gillespie, 2006). Spectral mixture analysis (SMA) has been developed as a method to transform the reflectance in the bands of multispectral images to fractions of reference endmembers, which are reflectance spectra of well-characterized materials that mix to produce spectra equivalent to those of pixels of interest in the image (Adams et al., 1995). As part of SMA techniques, linear spectral unmixing (LSU) models tread the radiation recorded by a sensor as the result of a linear mixture of spectrally pure endmember radiances (Small and Lu 2006). This method is based on the assumptions that: 1) the recorded radiation by the sensor for each pixel is limited to the sensor's IFOV, and assumes no influences by reflected radiation from neighbouring pixels (Settle and Drake 1993), 2) the overall global radiance is proportional to the surface occupied by each land cover type, and 3) the spectrally pure endmembers are valid for the whole study area (Quarmby et al. 1992). LSU models describe radiation reflected by an individual pixel (*i,j*) of a band *k* as the result of the product of reflectance for each land cover type by their respective mixture fraction plus an additional associated error for each pixel. The general expression of the model is presented in the following equation:

$$\rho_{i,j,k} = \sum_{m=1,p} F_{i,j,m}\ \rho_{m,k} + e_{i,j} \tag{2}$$

Where $\rho_{i,j,k}$ is the observed reflectance of a pixel for row *i*, column *j*, and band *k* ; $F_{i,j,m}$ is the proportion of component *m* of a pixel for row *i*, column *j*, for each one of the pure components; $\rho_{m,k}$ is the characteristic reflectance for component *m* in band *k* ; and $e_{i,j}$ is the

error associated to the estimation of proportions for each pixel *i*, *j*. The Least Square Mixing Model proposed by Shimabukuro and Smith (1991) is commonly used to resolve linear spectral mixture models. The method proposed by Shimabukuro and Smith (1991) assumes two initial restrictions for the computation of the proportions of spectrally pure endmembers. The first one implies that pure endmember proportions must range between 0 and 1. This means that the proportions of the components are normalized to a common range of potential values. The following expression summarizes this first restriction:

$$0 \leq F_{i,j,m} \leq 1 \tag{3}$$

The second restriction is that the sum of the fractions for every component is equal to the total pixel surface. In this way, it is quite simple to express the individual contribution or fraction of an endmember in relation to the total reflectance of the pixel.

$$\sum_{m=1,p} F_{i,j,m} = 1 \tag{4}$$

The choice of a LSU model must consider both the landscape of the test site and the ability of the model to depict the structure, shape and distribution of the basic landscape components (Ferreira et al. 2007). Well-chosen endmembers not only represent materials found in the scene, but provide an intuitive basis for understanding and describing the information in the image (Adams and Gillespie 2006). Endmembers were obtained after applying a spatial and spectral remote sensing data dimensionality reduction with the minimum noise fraction (MNF) and pixel purity index (PPI) techniques, respectively. The MNF is used to detect the inherent dimensionality of image data, segregating noise from the signal in the data and reducing computational requirements for subsequent processing tasks (Boardman and Kruse, 1994). The MNF as modified from Green et al. (1988) consists in two steps: 1) applying a transformation, based on an estimated noise covariance matrix to decorrelate and rescale the noise in the data (noise has unit variance and no band-to-band correlations); and 2) performing a standard principal component transformation of the noise-whitened data. A final dataset of coherent and almost noise-free bands are selected from the MNF output and can be used for subsequent processing steps. Pixel Purity Index (PPI) is a procedure for finding the most spectrally pure (extreme) pixels that typically correspond to mixing endmembers in multispectral and hyperspectral images (ITT VIS, 2008). PPI is computed by repeatedly projecting *n*-dimensional scatterplots onto a random unit vector; the extreme pixels in each projection (those pixels that fall onto the ends of the unit vector) are recorded and the total number of times each pixel is marked as extreme is noted. The selection of extreme pixels corresponding to analogous surface features is complex due to the great number of pixels typically found in remote sensing image data. The *n*-dimensional visualizer implemented in ENVI software (ITT Visual Information Solutions) is a tool to locate, identify, and cluster the purest pixels and most extreme spectral responses in a data set. The distribution of these points in *n*-space can be used to estimate the number of spectral endmembers and their pure spectral signatures (Boardman, 1993). Three endmembers were used in the LSU model of the study area, namely green vegetation (GV), non-photosynthetic vegetation (NPV) and shade (S). The GV endmember represents the signature of green dense vegetation, the NPV endmember is the signature of bare soil or sparse non-photosynthetic vegetation, and the shade endmember represents the signature of dark pixels and water bodies.

2.6 Statistical methods

The possible existence of differences in soil properties based on the land cover classes was determined by the use of the analysis of variance (ANOVA). ANOVA is used to evaluate significant differences between means of independent variables. The observed variance of independent variables is partitioned into components by several explanatory variables (factors). Land cover class was the factor employed in the analysis. Post-hoc analysis was performed using Tukey method.

Relationships between fraction endmembers and soil properties were studied by the principal component analysis (PCA). PCA is a technique of data dimensionality reduction that performs an orthogonal transformation to convert potentially correlated input variables into uncorrelated variables or principal components. The first components accumulate most of the variance and therefore, the most useful information about the variables.

Regression analyses between soil properties and fraction endmembers were performed for quantitative estimation of soil properties. A linear regression analysis applying a stepwise method for variable entry and removal was the selected statistical technique. Model selection was based on the lower typical error of the estimation and minimum collinearity.

3. Results and discussion

The relationship between various soil properties and land cover classes was analysed. Two approaches to the study of land cover are presented. A first categorization based on discrete land cover classes and another based on mixture fractions. Finally, statistical models for predicting soil properties of interest in the study of soil salinity through the use of mixture fractions are presented.

3.1 Soil properties

The study was focused on soil electrical conductivity (EC), pH and organic carbon (OC) (Table 2). These properties are important in chemical and biological quality of soils (Lal et al., 1999). Previous studies in semiarid areas combining remote sensing and soil analyses have indicated significant differences in these properties in different land cover classes (Biro et al.,

Land covers	EC (mS/cm)	pH	OC (%)
Arable land	1.38 ± 1.01 *ab*	8.23 ± 0.26 *ab*	1.92 ± 0.85 *a*
Permanent crops	0.70 ± 1.00 *b*	8.40 ± 0.26 *b*	1.29 ± 0.24 *a*
Fallow/abandoned	3.52 ± 2.43 *ac*	8.14 ± 0.25 *ab*	1.46 ± 0.36 *a*
Saltmarsh	3.98 ± 2.86 *c*	8.05 ± 0.07 *ab*	3.61 ± 0.81 *b*
Palm groves	3.82 ± 2.42 *ac*	8.20 ± 0.20 *ab*	2.11 ± 1.00 *a*
Marsh	4.71 ± 2.04 *c*	7.82 ± 0.09 *a*	5.24 ± 1.39 *c*
P-value	<0.001***	<0.001***	<0.001***

Table 2. Descriptive statistics (mean ± standard deviation) of soil properties based on land cover classes. The *p*-value and homogeneous subgroups (lower case letters; Tukey test, $P < 0.05$) resulting from the ANOVA test are included.

2011). Cultivated areas (i.e. arable land and permanent crops, homogenous subgroup *b*) have lower electrical conductivity values than natural or semi-natural vegetation. The construction of drainage systems at agricultural areas to encourage the leaching for salinity control has been a traditional amelioration strategy (Qadir et al., 2000). This fact explains that marshes and saltmarshes soils have higher EC values than the other land cover classes, since they are areas with poor drainage and temporally flooded. Salinity increases when farming finishes (i.e. fallow/abandoned) because irrigation water is not available to promote salts leaching.

The pH values were slightly alkaline but significantly different for marshes. Wetland soils are characterized by the permanent or seasonal inundation of the land, promoting anaerobic conditions and thus reduced redox conditions (high concentration of H^+ which implies low pH)(Reddy et al., 2000). The organic carbon content was also different depending on the type of land cover. Arable land and permanent crops soils have organic carbon content ranging from 1.46 to 2.11% that is not very high (Pérez-Sirvent et al., 2003). Opposite, wetland soils (i.e. stable saltmarshes and saltmarshes) exhibited the highest organic carbon contents. Compared to upland areas, most wetland soils show an accumulation of organic matter by the higher rates of photosynthesis in wetlands than other ecosystems and the lower rates of decomposition due to anaerobic conditions (Reddy et al., 2000).

All soil properties are significantly correlated ($P<0.01$) according to the Pearson bivariate correlation test applied to the full dataset. Figure 3 shows two scatterplots of the land cover classes average values (error bars represent the standard deviation) of pH and organics carbon versus electrical conductivity (EC). EC is negatively correlated with pH (R=-0.61) and positively correlated with organic carbon (R=0.34), while pH and organic carbon are negatively correlated (R=-0.32). Two sets of distinct land uses mainly dependent on the EC values are distinguished: 1) active cultures: with low EC and OC values, and 2) natural vegetation and crops of low requirements (palm groves): with high EC and OC values, increasing as the land cover is more similar to the wetland. Palm groves are the most halotolerant crop and require little tillage.

3.2 Land cover classification

A land cover map was obtained with the *k*-nearest-neighbours algorithm (Figure 4). Optimum results were obtained with $k=4$. The area occupied by the land cover classes (hectares and percentage of the total area) was quantified (Table 3).

The study area is mainly agricultural but largely occupied by urban areas. Urban/man-made areas represent 14.4% of the study area. There is a clear distinction between the northeast portion (area between the two natural parks and the *Sierra del Molar*) with large fields and less presence of buildings, and the rest of the study area, with numerous buildings scattered, villages, small-size towns and smaller parcels. Dominant land cover classes are also different at these two sectors. Close to the natural parks, there are many saltmarshes (7.09% of the study area), marshes (1.95% of the study area), palm groves (2.21% of the study area) and arable land (45.76% of the area and mainly forage, barley and melons). The other sector has a massive presence of permanent crops (16.3% of the study area and mainly citrus trees such as orange and lemon trees).

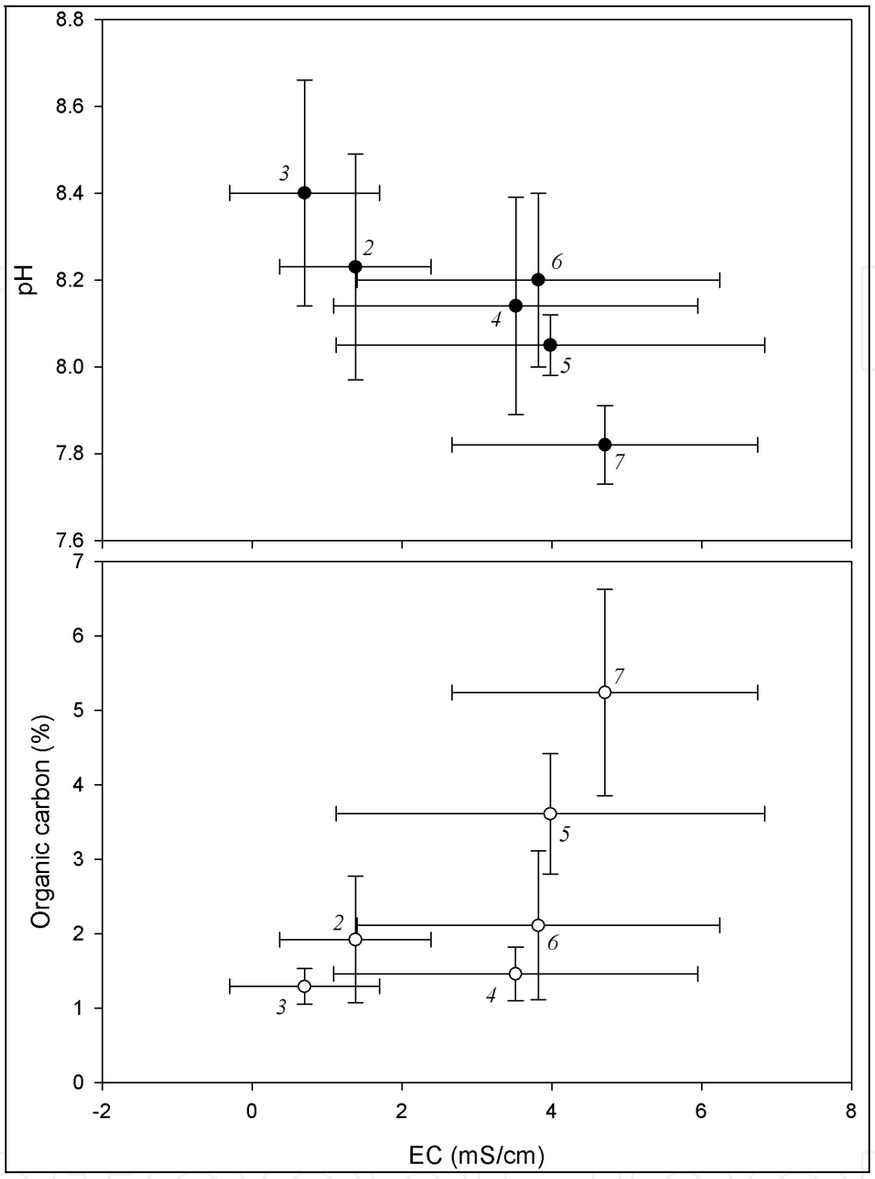

Fig. 3. Scatterplots with the average values pH and organic carbon versus electrical conductivity for land cover classes (numbers in italics are the ID number of the class). X and Y bars represent one standard deviation.

The distribution of land cover classes can be explained by the characteristics of the soils. Generally, the closest soils to the wetland areas of the natural parks are more saline. These soils have a poor drainage due to its lower altitude and very high-water tables, largely due to the horizontal flow of water and salts from the nearby water bodies. Permanent crops class dominates in areas that are close to the towns, being better drained and less saline. Fallow/abandoned areas (12.11% of the study area) are spread throughout the study area as a result of the abandonment of farming on individual fields. However, abandoned land is more present in the proximal portion of the natural parks since the conditions of salinization of soils led to their abandonment.

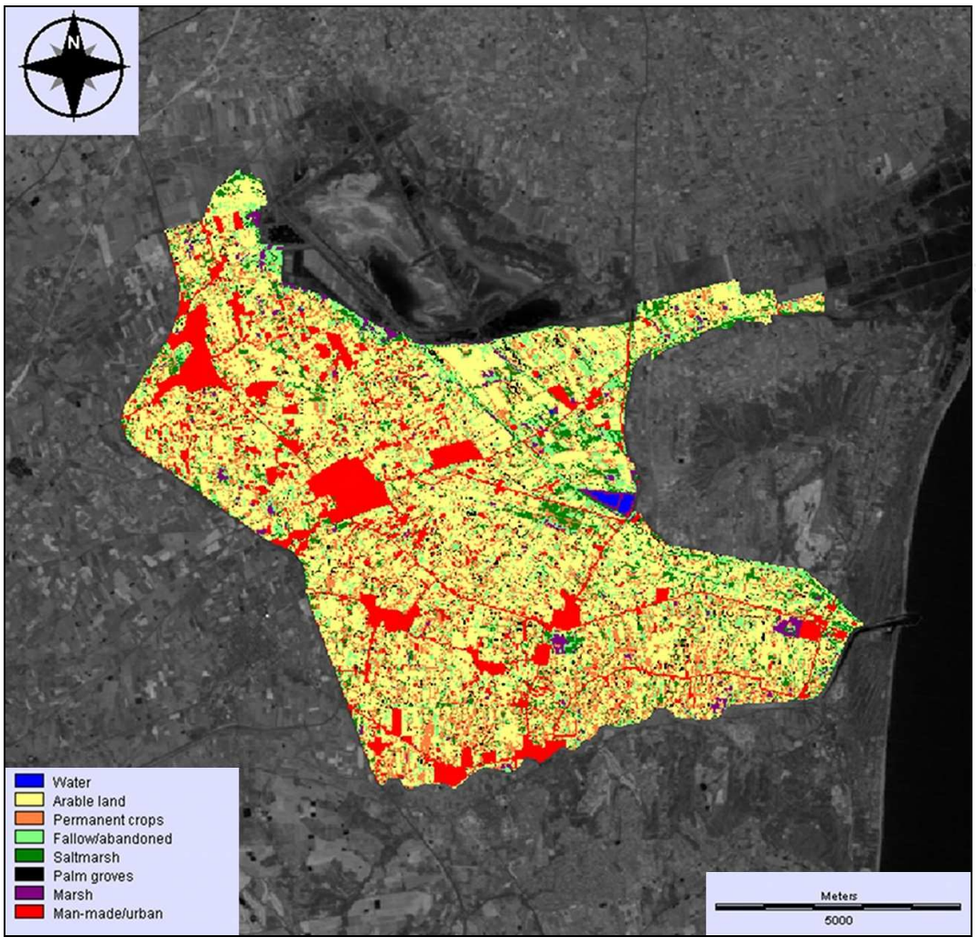

Fig. 4. Land cover map of the study area.

Land cover classes	Area (ha)	Area (%)
Water	17.37	0.20
Arable land	4061.52	45.76
Permanent crops	1446.93	16.30
Fallow/abandoned	1074.51	12.11
Saltmarsh	629.01	7.09
Palm groves	196.02	2.21
Marsh	172.71	1.95
Man-made/urban	1277.73	14.40
TOTAL	*8875.80*	*100*

Table 3. Area occupied by land cover classes according to the map obtained by k-nearest neighbour.

The land cover map accuracy was evaluated with the data set of validation points. Overall accuracy was a 68%, and KHAT value was 0.56. According to Landis and Koch (1977),

KHAT values ranging from 0.4 to 0.8 exhibit a moderate agreement. Inter-class confusion was detected analysing the error matrix. A portion of arable land (78% of producer's accuracy, 65% of user's accuracy) was wrongly classified as permanent crops, fallow/abandoned land or saltmarshes. A great portion of palm groves (21% of producer's accuracy and 75% of user's accuracy) was classified as arable land. The performance of the automatic classification for marshes (90% of producer's accuracy and 75% of user's accuracy) and water areas (100% of producer's accuracy and 80% of user's accuracy) was highly satisfactory. The performance of the KNN algorithm for our land cover classification approach was enough good and comparable with the accuracy obtained by Franco-Lopez et al. (2001) classifying a forest stand (52% of overall accuracy with k=10), and the results of the experiment carried on by Samaniego and Schulz (2009) classifying crop types (47% of overall accuracy with k=5).

3.3 Spectral unmixing and land covers

Spectral mixture analysis was applied to obtain fraction images of green vegetation (GV), non-photosynthetic vegetation (NPV) and shade endmembers. Spectral signatures of selected endmembers are highly distinctive (Figure 5). These endmembers had optimal spectral separability as measured with the transformed divergence method. GV endmember is associated with vigorous vegetation, NPV endmember is associated with bare soil and dry halophytic vegetation, and shade endmember is associated with water bodies and low illuminated areas.

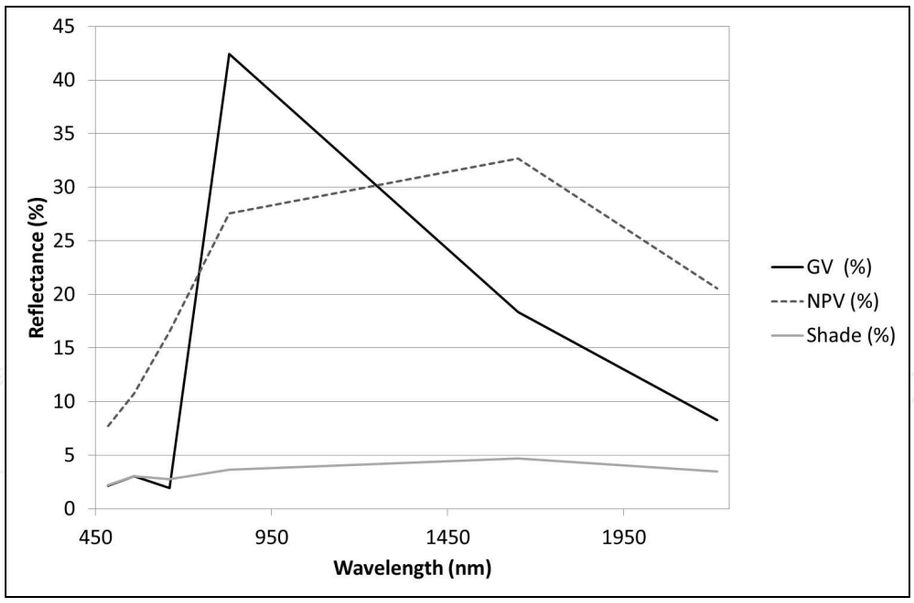

Fig. 5. Plot showing the spectral signatures of selected green vegetation (GV), non-photosynthetic vegetation (NPV) and shade endmembers.

Fraction images of the three endmembers and the residual fraction of the spectral mixture analysis were obtained (Figure 6). Values range from 0 for low high membership to the image fraction (black colour) to 1 for high membership (white colour). Fractions images are continuous variables that are graphically represented with a greyscale colour ramp. High

values of the shade fraction image are present in the wetland areas of the natural parks and in a triangular area in the middle-right boundary of the study area that corresponds with a small wetland. A white area in the right of the image corresponds with the Mediterranean Sea. High green vegetation fraction values area scattered through the study area. They correspond with active crops at the time of the image acquisition. Indeed, the white areas in the NPV image fraction correspond with bare soil and saltmarshes which vegetation is quite dry in summer and have a great spectral confusion with background soil. Urban areas were also associated with this fraction image. Finally, high values of the residual fraction are located in industrial areas, whose spectral signature was notably different respect to the three endmembers of the unmixing model.

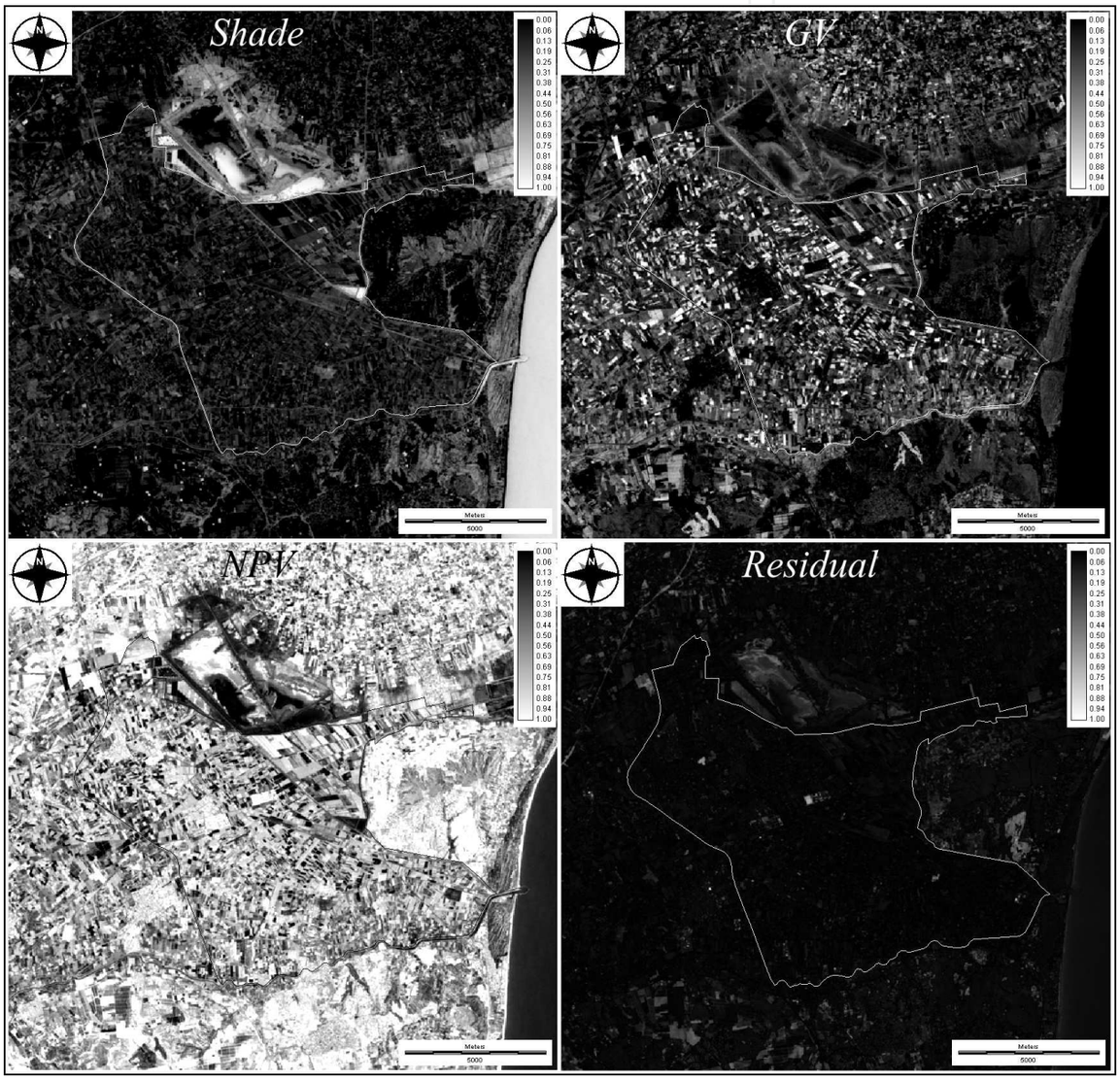

Fig. 6. Fraction images of shade/water, green vegetation (GV), non-photosynthetic vegetation (NPV) and the residual component of the linear spectral mixture analysis. White/black polygon represents the boundary of the study area.

Average values of the three fraction images for the land covers were computed and represented in a ternary diagram (Figure 7). Water land cover has high shade fraction values (>90%) and very low values for the GV and NPV fractions. Marshes have an important fraction of shade (>55%) and around 30% of the GV fraction. This mixture composition is highly indicative of the marshes structure with green *Phragmites australis* stands, growing on flooded or water-saturated soils. Shade fraction has a low contribution in the other land covers (<30%). Saltmarshes, permanent crops, arable land, fallow/abandoned and palm groves land cover classes have GV fraction values between 20-40% and NPV fraction values between 50-70%. This relative homogeneity in the mixture fractions values for different land cover classes could be attributed to the lower water availability in summer, that promotes a drying and browning of the vegetation and promotes spectral confusion. Melendez-Pastor et al. (2010b) previously observed this phenomenon in the study area. They also employed ternary diagrams, combining mixture fraction and land cover classes for a drought year and an average year. Soil or NPV fractions increase their contribution in a dry weather scenario (i.e. drought or summer) and the water and GV fractions have a lower contribution.

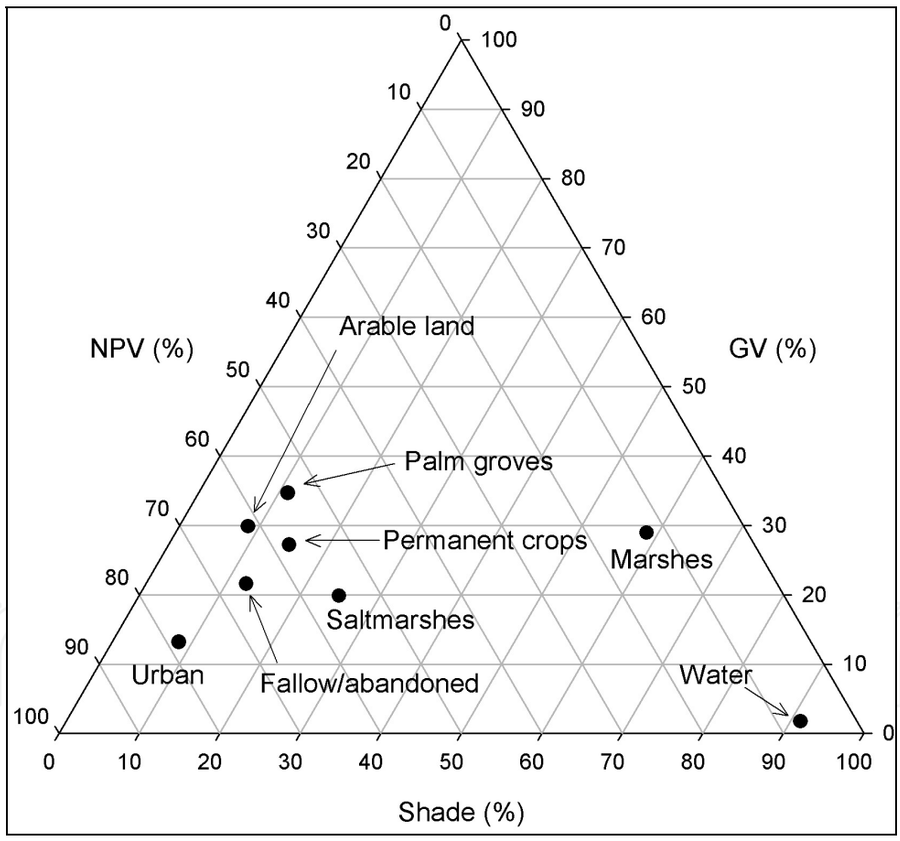

Fig. 7. Ternary diagram of the average mixture fraction values for the land cover classes.

3.4 Fraction endmembers to predict soil properties

Mixture fraction values were statistically related to soil salinity. Principal component analysis provided valuable information about the relationship among soil properties and spectral mixture analysis fractions. The first three principal components accumulated 75.8%

of total variance. PC1 was positively correlated with NPV fraction (factor loading = 0.988) and negatively correlated with GV fraction (factor loading = -0.902). PC1 might be used to separate vegetated from non-vegetated pixels. PC2 was positively correlated with electrical conductivity (factor loading = 0.778) and the shade fraction (factor loading = 0.604) and negatively correlated with the pH (factor loading = -0.785). PC2 might be used to differentiate soil salinity status.

Salinization status seems to be related to the abundance of the shade fraction. This result could be explained by the presence of water at the soil profile, which is an evidence of poor drainage that could lead to salt accumulation. Thus, monitoring shade fraction values along a year could be an indirect method to detect the evolution of soil electrical conductivity with remote sensing. PC3 was positively correlated with the residual fraction of the spectral unmixing (factor loading = 0.853) and organic carbon content (factor loading = 0.711). Evident negative correlations with the PC3 were not found.

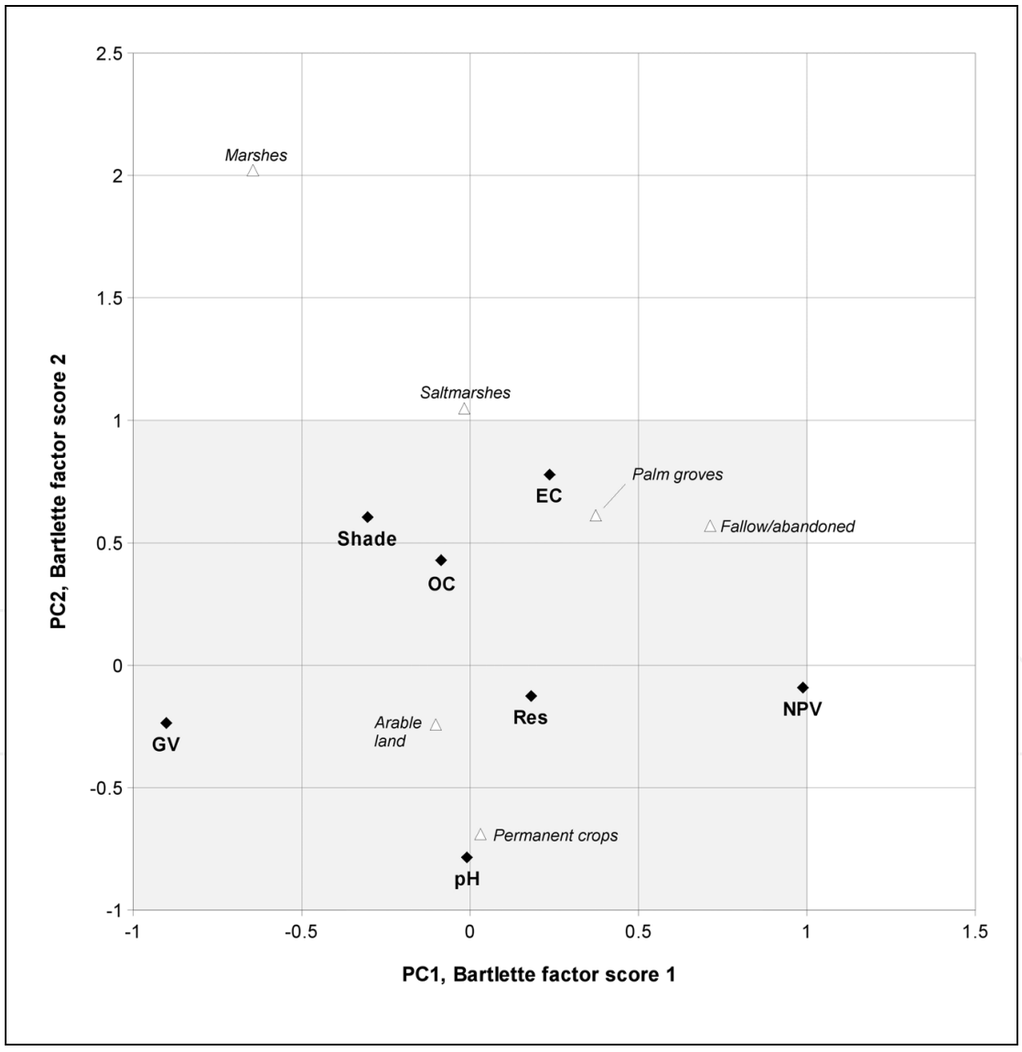

Fig. 8. Factor loadings plot for the measured soil properties and mixture fractions, and average values factor scores plot for the land cover classes.

Previous studies assessed the relationships between PC factor loadings of soil properties and PC factor scores of land cover classes (Biro et al., 2011). We also included the mixture fraction values for soil plots in the principal component analysis. Soil properties and mixture fractions factor loadings and average factor scores for land cover classes of the first two components were plotted to explore their relationship (Figure 8). Factor loading values range from -1 to 1. Factor scores of land cover classes were also included in the plot. Land cover classes were differentiated from each other along PC1, mainly because of the high positive factor loading of the NPV fraction and high negative factor loading of the GV fraction. Also, land cover classes were differentiated from each other along PC2, mainly because of the high positive loadings of the shade fraction, electrical conductivity and organic carbon content, and high negative loading value of pH.

Finally, we tested the usefulness of mixture fractions to predict EC. Stepwise linear regression was employed to model relationship among EC and mixture fractions. EC variable was normalised with the natural logarithm, while the other variables were normal. Table 4 summarizes the main parameters of two linear regression models. Moderate adjustment was obtained from the regression with R=0.338 for the first model and R=0.408 for the second model. The ANOVA test (data not included in the table) indicated the usefulness of the models with a *p*-value <0.001 for both cases. Model 1 included GV fraction as the unique mixed fraction predictor variable, while model 2 included GV and also the shade fraction. In both models, the coefficient B has a negative value for the variable GV, suggesting an inverse relationship between the green covers and EC. By contrast, the regression coefficient B was positive for the shade fraction, indicating a direct relationship between the presence of shadows/water and EC. This latter observation corroborates the interpretation given in the principal component analysis on the usefulness of the shade fraction to predict soil salinity. Collinearity statistics revealed the absence of collinearity problems as we obtained tolerance values much greater than 0 and VIF values much lower than 15 (SPSS, 2009).

Model	R	R^2	Adjusted R^2	Predictors	Unstandardized Coefficients		Sig.	Collinearity Statistics	
					B	Std. Error		Tolerance	VIF
1	0.338	0.115	0.107	(Constant)	7.483	0.106	0.000		
				GV	-1.081	0.279	0.000	1.000	1.000
2	0.408	0.167	0.152	(Constant)	7.302	0.123	0.000		
				GV	-1.005	0.273	0.000	0.989	1.011
				Shade	1.320	0.492	0.008	0.989	1.011

VIF: variable inflation factor

Table 4. Summary of results of linear regression models.

Regression models with mixture fractions did not show collinearity that could lead us to false predictions. A major constraint using proximal and remote sensing data for mapping salinity is related to the fact that there is a strong vertical, spatial and temporal variability of salinity in the soil profile (Mulder et al., 2011). Direct and precise estimation of the salt quantities is difficult by using satellite data with a low spectral resolution because these fail

to detect specific absorption bands of some salt types, and the spectra interfere with other soil chromophores (Mougenot et al., 1993). More research will help to improve the prediction of soil properties with remote sensing data for a fast assessment of soil status over large areas and at low cost.

4. Conclusions

This chapter provides an interesting case of study on the application of remote sensing to soil salinity. The land use and management greatly affect soil salinity and land cover mapping helps to delineate areas with different severity of salinization. The use of spectral mixture analysis in combination with land cover maps and soil properties data is a more advanced technique. Mixture fractions help to know the spectral behaviour of land cover and their constituents using a simple three endmembers model. In addition, mixture fractions can be used as predictors in regression models to predict the electrical conductivity of soils. The results of regression models were encouraging but require further research to improve them. Since mixture fractions are sensitive to spectral changes due to changes in ground surface, they may be particularly useful for mapping the severity of soil salinization processes over time with low coast satellite images. The combined use of soil properties analytics, land cover maps and spectral mixture analysis is feasible for monitoring saline soils and land management over large areas with a reduced cost.

5. Acknowledgment

The authors acknowledge the Spanish Ministry of Science and Innovation for the financial support of the project '*Efectos de la aplicación de un compost de biosólido sobre la calidad de suelos con distinto grado de salinidad*' with the reference CGL2009-11194 that allowed this research.

6. References

Acosta, J.A.; Faz, A.; Jansen, B.; Kalbitz, K. & Martínez-Martínez, S. (2011). Assessment of salinity status in intensively cultivated soils under semiarid climate, Murcia, SE Spain. *Journal of Arid Environments*, Vol. 75, No. 11 (November 2011), pp. 1056-1066, ISSN 0140-1963

Adams, J.B. & Gillespie, A.R. (2006). *Remote Sensing of Landscapes with Spectral Images. A Physical Modeling Approach*. Cambridge University Press, ISBN 0521662214, Cambridge, UK

Adams, J.B.; Sabol, D.E.; Kapos, V.; Filho, R.A.; Roberts, D.A.; Smith, M.O. & Gillespie, A.R. (1995). Classification of Multispectral Images Based on Fractions of Endmembers: Application to Land-Cover Change in the Brazilian Amazon. *Remote Sensing of Environment*, Vol. 52, No. 2 (May 1995), pp. 137-154, ISSN 0034-4257

Ardahanlioglu, O.; Oztas, T.; Evren, S.; Yilmaz, H. & Yildirim, Z.N. (2003). Spatial variability of exchangeable sodium, electrical conductivity, soil pH and boron content in salt- and sodium-affected areas of the Igdir plain (Turkey). *Journal of Arid Environments*, Vol. 54, No. 3 (July 2003), pp. 495-503, ISSN 0140-1963

Ben-Dor, E. & Banin, A. (1994). Visible and near-infrared (0.4-1.1 μm) analysis of arid and semiarid soils. *Remote Sensing of Environment*, Vol. 48, No. 3 (June 1994), pp. 261-274, ISSN 0034-4257

Ben-Dor, E.; Inbar, Y. & Chen, Y. (1997). The reflectance spectra of organic matter in the visible near-infrared and short wave infrared region (400–2500 nm) during a controlled decomposition process. *Remote Sensing of Environment*, Vol. 61, No. 1 (July 1997), pp. 1-15, ISSN 0034-4257

Ben-Dor, E.; Chabrillat, S.; Demattê, J.A.M.; Taylor, G.R.; Hill, J.; Whiting, M.L. & Sommer, S. (2009). Using Imaging Spectroscopy to study soil properties. *Remote Sensing of Environment*, Vol. 113, No. SUPPL. 1 (September 2009), pp. S38-S55, ISSN 0034-4257

Biro, K.; Pradhan, B.; Buchroithner, M. & Makeschin, F. (2011). Land use/land cover change analysis and its impact on soil properties in the Northern Part of Gadarif Region, Sudan. *Land Degradation & Development*, Vol. in press DOI: 10.1002/ldr.1116, ISSN 1085-3278

Blanzieri, E. & Melgani, F. (2008). Nearest Neighbor Classification of Remote Sensing Images With the Maximal Margin Principle. *IEEE Transactions on Geoscience and Remote Sensing*, Vol. 46, No. 6 (June 2008), pp. 1804-1811, ISSN 0196-2892

Blázquez, A.M. (2003). *L'Albufera d'Elx: evolución cuaternaria y reconstrucción paleoambiental a partir del estudio de los foraminíferos fósiles*. PhD dissertation. Universitat de Valencia, Valencia, Spain.

Boardman, J.W. (1993). Automating Spectral Unmixing of AVIRIS Data Using Convex Geometry Concepts, *Summaries of the Fourth Annual JPL Airborne Geosciences Workshop, Volume 1: AVIRIS Workshop, JPL Publication 93-26*, pp. 11-14. Washington D.C., USA.

Boardman, J.W. & Kruse, F.A. (1994). Automated spectral analysis: A geological example using AVIRIS data, northern Grapevine Mountains, Nevada. *Proceedings, Environmental Research Institute of Michigan (ERIM) Tenth Thematic Conference on Geologic Remote Sensing*, pp. I-407 - I-418. Ann Arbor (MI), USA.

Caravaca, F.; Masciandaro, G. & Ceccanti, B. (2002). Land use in relation to soil chemical and biochemical properties in a semiarid Mediterranean environment. *Soil and Tillage Research*, Vol. 68, No. 1 (October 2002), pp. 23-30, ISSN 01671987

Chander, G. & Markham, B. (2003). Revised Landsat-5 TM Radiometric Calibration Procedures and Postcalibration Dynamic Ranges. *IEEE Transactions on Geoscience and Remote Sensing*, Vol. 41, No. 11 PART II, (November 2003), pp. 2674-2677, ISSN 0196-2892

Chander, G.; Haque, M.O.; Micijevic, E. & Barsi, J.A. (2010). A Procedure for Radiometric Recalibration of Landsat 5 TM Reflective-Band Data. *IEEE Transactions on Geoscience and Remote Sensing*, Vol. 48, No. 1 (January 2010), pp. 556-574, ISSN 0196-2892

Chavez Jr, P.S. (1989). Radiometric calibration of Landsat Thematic Mapper multispectral images. *Photogrammetric Engineering & Remote Sensing*, Vol. 55, No. 9 (September 1989), pp. 1285 -1294, ISSN 0099-1112

Chavez Jr, P.S. (1996). Image-based atmospheric corrections - Revisited and improved. *Photogrammetric Engineering & Remote Sensing*, Vol. 62, No. 9 (September 1996), pp. 1025-1036, ISSN 0099-1112

Clark, R.N. (1999). Chapter 1: Spectroscopy of Rocks and Minerals, and Principles of Spectroscopy. In: *Manual of Remote Sensing, Volume 3, Remote Sensing for the Earth Sciences*, A.N. Rencz, (Ed.), pp. 3-58. John Wiley and Sons, ISBN 0471294055, New York, USA

Cohen, J. (1960). A Coefficient of Agreement for Nominal Scales. *Educational and Psychological Measurement*, Vol. 20, No. 1 (April 1960), pp. 37-46. ISSN 0013-1644

Congalton, R.G. (2004). Putting the map back in map accuracy assessment. In: *Remote Sensing and GIS accuracy assessment*, R.S. Lunetta & J.G. Lyon, (Eds.), pp. 1-11. CRC Press, ISBN 156670443X, Boca Raton (FL), USA

Congalton, R.G.; Oderwald, R.G. & Mean, R.A. (1983). Assessing Landsat Classification Accuracy Using Discrete Multivariate Analysis Statistical Techniques. *Photogrammetric Engineering & Remote Sensing*, Vol. 49, No. 12 (December 1983), pp. 1671-1678, ISSN 0099-1112

Csillag, F.; Pasztor, L. & Biehl, L.L. (1993). Spectral band selection for the characterization of salinity status of soils. *Remote Sensing of Environment*, Vol. 43, No. 3 (March 1993), pp. 231-242, ISSN 0034-4257

Dalsted, K.J.; Worcester, B.K. & Brun, L.J. (1979). Detection of Saline Seeps by Remote Sensing Techniques. *Photogrammetric Engineering & Remote Sensing*, Vol. 45, No. 3 (March 1979), pp. 285-291, ISSN 0099-1112

Dehaan, R.L. & Taylor, G. R. (2002). Field-derived spectra of salinized soils and vegetation as indicators of irrigation-induced soil salinization. *Remote Sensing of Environment*, Vol. 80, No. 3 (June 2002), pp. 406-417, ISSN 0034-4257

Dehaan, R.L. & Taylor, G.R. (2003). Image-derived spectral endmembers as indicators of salinisation. *International Journal of Remote Sensing*, Vol. 24, No. 4 (February 2003), pp. 775-794, ISSN 0143-1161

De Martonne, E. (1926). L'indice d'aridité. *Bulletin de l'Association des geógraphes français*, Vol. 9, pp. 3-5, ISSN 0004-5322

De Paz, J.M.; Sánchez, J. & Visconti, F. (2006). Combined use of GIS and environmental indicators for assessment of chemical, physical and biological soil degradation in a Spanish Mediterranean region. *Journal of Environmental Management*, Vol. 79, No. 2 (April 2006), pp. 150-62, ISSN 03014797

Dutkiewicz, A.; Lewis, M. & Ostendorf, B. (2009). Evaluation and comparison of hyperspectral imagery for mapping surface symptoms of dryland salinity. *International Journal of Remote Sensing*, Vol. 30, No. 3 (February 2009), pp. 693-719, ISSN 0143-1161

Dwivedi, R.S.; Ramana, K.V.; Thammappa, S.S. & Singh, A. N. (2001). The Utility of IRS-1C LISS-Ill and PAN-Merged Data for Mapping Salt-Affected Soils. *Photogrammetric Engineering & Remote Sensing*, Vol. 67, No. 10 (October 2001), pp. 1167-1175, ISSN 0099-1112

European Commission. (2002). *Towards a Thematic Strategy for Soil Protection. COM(2002) 179 final*. European Commission, Brussels, Belgium.

European Commission. (2003). *Extent, causes, pressures, strategies and actions that should be adopted to prevent and to combat salinization and sodification in Europe*. Directorate General Environment, Directorate B, Erosion Working Group (Task 5; Topic: Salinization and Sodification), Brussels, Belgium.

FAO. (2002). *Crops and Drops, making the best use of water for agriculture*, Food and Agriculture Organization of the United Nations, Rome, Italy.

Farifteh, J.; Van Der Meer, F.; Van Der Meijde, M. & Atzberger, C. (2008). Spectral characteristics of salt-affected soils: A laboratory experiment. *Geoderma*, Vol. 145, No. 3-4 (June 2008), pp. 196-206, ISSN 0016-7061

Ferreira, M.E.; Ferreira, L.G.; Sano, E.E. & Shimabukuro, Y.E. (2007). Spectral linear mixture modelling approaches for land cover mapping of tropical savanna areas in Brazil. *International Journal of Remote Sensing*, Vol. 28, No. 2 (January 2007), pp. 413-429, ISSN 0143-1161

Foody, G.M. (2002). Status of land cover classification accuracy assessment. *Remote Sensing of Environment*, Vol. 80, No. 1 (April 2002), pp. 185-201, ISSN 0034-4257

Franco-Lopez, H.; Ek, A.R., & Bauer, M.E. (2001). Estimation and mapping of forest stand density, volume, and cover type using the k-nearest neighbors method. *Remote Sensing of Environment*, Vol. 77, No. 3 (September 2001), pp. 251-274, ISSN 0034-4257

Ghrefat, H.A. & Goodell, P.C. (2011). Land cover mapping at Alkali Flat and Lake Lucero, White Sands, New Mexico, USA using multi-temporal and multi-spectral remote sensing data. *International Journal of Applied Earth Observations and Geoinformation*, Vol. 13, No. 4 (August 2011), pp. 616-625, ISSN 0303-2434

Green, A.A.; Berman, M.; Switzer, P. & Craig, M.D. (1988). A transformation for ordering multispectral data in terms of image quality with implications for noise removal. *IEEE Transactions on Geoscience and Remote Sensing*, Vol. 26, No. 1 (January 1988), pp. 65-74, ISSN 0196-2892

Haapanen, R.; Ek, A.R.; Bauer, M.E. & Finley, A.O. (2004). Delineation of forest/nonforest land use classes using nearest neighbor methods. *Remote Sensing of Environment*, Vol. 89, No. 3 (February 2004), pp. 265-271, ISSN 0034-4257

Hernández Bastida, J.A.; Vela de Oro, N. & Ortiz Silla, R. (2004). Electrolytic Conductivity of Semiarid Soils (Southeastern Spain) in Relation to Ion Composition. *Arid Land Research and Management*, Vol. 18, No. 3 (July 2004), pp. 265-281, ISSN 15324982

Howari, F.M., Goodell, P.C. & Miyamoto, S. (2000). Spectral properties of salt crusts formed on saline soils. *Journal of Environmental Quality*, Vol. 31, No. 5 (September 2002), pp. 1453-61, ISSN 00472425

ITT VIS. (2008). *ENVI 4.5 User's Guide*. ITT Visual Information Solutions Boulder (CO), USA.

Jensen, J.R. (2005). *Introductory Digital Image Processing* (3rd Edition). Prentice Hall, ISBN 0131453610, Upper Saddle River (NJ), USA

Jensen, J. R. (2007). *Remote Sensing of the Environment: An Earth Resource Perspective* (2nd edition), Pentice Hall, ISBN 0131889508, Upper Saddle River (NJ), USA

Kaufman, Y.J. (1989). The atmospheric effect on remote sensing and its corrections. In: *Theory and Applications of Optical Remote Sensing*, G. Asrar, (Ed.), pp. 336-428, Wiley-Interscience, ISBN 0471628956, New York, USA

Lal, R., Mokma, D. & Lowery, B. (1999). Relation between soil quality and erosion. In: *Soil quality and soil erosion*, R. Lal, (Ed.), pp. 237-258, CRC Press, ISBN 1574441000, Boca Raton (FL), USA

Landis, J.R. & Koch, G. G. (1977). The measurement of observer agreement for categorical data. *Biometrics*, Vol. 33, No. 1 (March 1977), pp. 159-174, ISSN 0006341X

Lillesand, T.M.; Kiefer, R.W. & Chipman, J.W. (2003). *Remote Sensing and Image Interpretation* (5th edition). John Wiley and Sons, ISBN 9812530797, Hoboken (NJ), USA

Majaliwa, J.G.M.; Twongyirwe, R.; Nyenje, R.; Oluka, M.; Ongom, B.; Sirike, J.; Mfitumukiza, D.; Azanga, E.; Natumanya, R.; Mwerera, R. & Barasa, B. (2010). The Effect of Land Cover Change on Soil Properties around Kibale National Park in South Western Uganda. *Applied and Environmental Soil Science*, Article ID 185689, ISSN 1687-7667

Mather, P.M. (2004). *Computer Processing of Remotely-Sensed Images: An Introduction* (3rd edition). Wiley, ISBN 0470849185, Chichester, UK

Melendez-Pastor, I.; Navarro-Pedreño, J.; Koch, M., & Gómez, I. (2010). Applying imaging spectroscopy techniques to map saline soils with ASTER images. *Geoderma*, Vol. 158, No. 1-2 (August 2010), pp. 55-65, ISSN 0016-7061

Melendez-Pastor, I.; Navarro-Pedreño, J.; Koch, M., & Gómez, I. (2010). Multi-resolution and temporal characterization of land use classes in a Mediterranean wetland with land cover fractions. *International Journal of Remote Sensing*, Vol. 31, No. 20 (October 2010), pp. 5365-5389, ISSN 0143-1161

Mermut, A.R., & Eswaran, H. (2001). Some major developments in soil science since the mid-1960s. *Geoderma*, Vol. 100, No. 3-4 (May 2001), pp. 403 -426, ISSN 0016-7061

Metternicht, G.I. & Zinck, J.A. (2003). Remote sensing of soil salinity: Potentials and constraints. *Remote Sensing of Environment*, Vol. 85, No. 1 (April 2003), pp. 1-20, ISSN 0034-4257

Metternicht, G. & Zinck, J.A. (1997). Spatial discrimination of salt- and sodium-affected soil surfaces. *International Journal of Remote Sensing*, Vol. 18, No. 12 (June 1997), pp. 2571-2586, ISSN 0143-1161

Moran, M.S.; Jackson, R.D.; Slater, P.N. & Teillet, P.M. (1992). Evaluation of simplified procedures for retrieval of land surface reflectance factors from satellite sensor output. *Remote Sensing of Environment*, Vol. 41, No. 1-2 (August-September 1992), pp. 169-184. ISSN 0034-4257

Mougenot, B.; Pouget, M. & Epema, G.F. (1993). Remote sensing of salt affected soils. *Remote Sensing Reviews*, Vol. 7, No. 3-4, pp. 241-259, ISSN 02757257

Mulder, V.L.; De Bruin, S.; Schaepman, M.E. & Mayr, T. R. (2011). The use of remote sensing in soil and terrain mapping—A review. *Geoderma*, Vol. 162, No. 1-2 (April 2011), pp. 1-19, ISSN 0016-7061

Nelson, D.W. & Sommers, L. E. (1982). Total carbon, organic carbon, and organic matter. In: *Methods of Soil Analysis*. A.L. Page; R.H. Miller & D.R. Keeney (Eds.), pp. 539-579, American Society of Agronomy (ASA),Madison (WI), USA

Pérez-Sirvent, C.E.; Martínez-Sánchez, M.J.; Vidal, J. & Sánchez, A. (2003). The role of low-quality irrigation water in the desertification of semi-arid zones in Murcia, SE Spain. *Geoderma*, Vol. 113, No. 1-2 (April 2003), pp. 109-125, ISSN 0016-7061

Qadir, M.; Ghafoor, A., & Murtaza, G. (2000). Amelioration strategies for saline soils: A review. *Land Degradation & Development*, Vol. 11, No. 6 (November-December 2000), pp. 501-521, ISSN 1085-3278

Quarmby, N.A.; Townshend, J.R.G.; Settle, J.J.; White, K.H.; Milnes, M.; Hindle, T.L. & Silleos, N. (1992). Linear mixture modelling applied to AVHRR data for crop area estimation. *International Journal of Remote Sensing*, Vol. 13, No. 3 (February 1992), pp. 415-425, ISSN 0143-1161

Reddy, K.R.; D'Angelo, E.M. & Harris, W.G. (2000). Biogeochemistry of Wetlands. In: *Handbook of Soil Science*, M.E. Sumner, (Ed.), p. G-89-G-119, CRC Press, ISBN 0849331366, Boca Raton (FL), USA

Richards, L.A. (1954). *Diagnosis and improvement of saline and alkali soils. Agriculture Handbook No. 60*. United States Department of Agriculture (USDA), Washington D.C., USA.

Richardson, A.J.; Gerbermann, A.H.; Gausman, H.W. & Cuellar, J.A. (1976). Detection of Saline Soils with Skylab Multispectral Scanner Data. *Photogrammetric Engineering & Remote Sensing*, Vol. 42, No. 5 (May 1976), pp. 679-684, ISSN 0099-1112

SPSS (2009). *PSAW 18.0 for Windows Help System*. IBM Corpotation, Armonk (NY), USA

Samaniego, L. & Schulz, K. (2009). Supervised Classification of Agricultural Land Cover Using a Modified k-NN Technique (MNN) and Landsat Remote Sensing Imagery. *Remote Sensing*, Vol. 1, No. 4 (December 2009), pp. 875-895, ISSN 2072-4292

Schmid, T.; Koch, M. & Gumuzzio, J. (2009). Applications of hyperspectral imagery to soil salinity mapping. In: *Remote Sensing of Soil Salinization: Impact and Land Management*, G. Metternicht & J.A. Zinck, (Eds.), pp. 113-140. CRC Press, ISBN 1420065025, Boca Raton (FL), USA

Settle, J.J. & Drake, N.A. (1993). Linear mixing and the estimation of ground cover proportions. *International Journal of Remote Sensing*, Vol. 14, No. 6 (March 1993), pp. 1159-1177, ISSN 0143-1161

Shimabukuro, Y.E. & Smith, J.A. (1991). The least-squares mixing models to generate fraction images derived from remote sensing multispectral data. *IEEE Transactions on Geoscience and Remote Sensing*, Vol. 29, No. 1 (January 1991), pp. 16-20, ISSN 0196-2892

Sitte, P.; Ziegler, H.; Ehrendorfer, F. & Bresinsky, A. (1994). *Strasburger. Tratado de Botánica* (8th Spanish edition), Omega, ISBN 8428209790, Barcelona, Spain

Small, C. & Lu, J.W.T. (2006). Estimation and vicarious validation of urban vegetation abundance by spectral mixture analysis. *Remote Sensing of Environment*, Vol. 100, No. 4 (February 2006), pp. 441-456, ISSN 0034-4257

Soil Survey Staff. (2006). *Keys to Soil Taxonomy* (10th Edition).United States Department of Agriculture (USDA), Washington D.C., USA

Song, C.; Woodcock, C.E.; Seto, K.C.; Lenney, M.P. & Macomber, S.A. (2001). Classification and Change Detection Using Landsat TM Data: When and How to Correct Atmospheric Effects? *Remote Sensing of Environment*, Vol. 75, No. 2 (February 2001), pp. 230-244, ISSN 0034-4257

Townsend, P.A. & Walsh, S.J. (2001). Remote sensing of forested wetlands: application of multitemporal and multispectral satellite imagery to determine plant community composition and structure in southeastern USA. *Plant Ecology*, Vol. 157, No. 2 (December 2001), pp. 129-151, ISSN 1385-0237

UNEP. (1997). *World Atlas of Desertification* (2nd edition). United Nations Environment Programme (UNEP), ISBN 0340691662, Nairobi, Kenya

Walkley, A. & Black, I.A. (1934). An Examination of the Degtjareff Method for Determining Soil Organic Matter, and A Proposed Modification of the Chromic Acid Titration Method. *Soil Science*, Vol. 37, No. 1 (January 1934), pp. 29-38, ISSN 0038-075X

Weng, Y.; Gong, P. & Zhu, Z. (2008). Reflectance spectroscopy for the assessment of soil salt content in soils of the Yellow River Delta of China. *International Journal of Remote Sensing*, Vol. 29, No. 19 (October 2008), pp. 5511-5531, ISSN 0143-1161

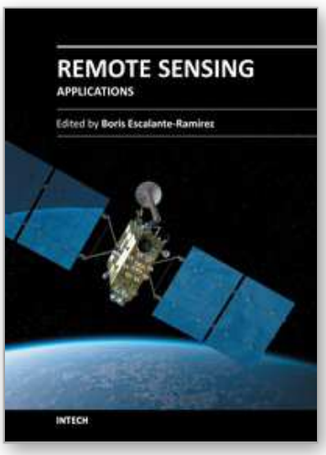

Remote Sensing - Applications
Edited by Dr. Boris Escalante

ISBN 978-953-51-0651-7
Hard cover, 516 pages
Publisher InTech
Published online 13, June, 2012
Published in print edition June, 2012

Nowadays it is hard to find areas of human activity and development that have not profited from or contributed to remote sensing. Natural, physical and social activities find in remote sensing a common ground for interaction and development. This book intends to show the reader how remote sensing impacts other areas of science, technology, and human activity, by displaying a selected number of high quality contributions dealing with different remote sensing applications.

How to reference
In order to correctly reference this scholarly work, feel free to copy and paste the following:

Ignacio Melendez-Pastor, Encarni I. Hernández, Jose Navarro-Pedreño and Ignacio Gómez (2012). Mapping Soil Salinization of Agricultural Coastal Areas in Southeast Spain, Remote Sensing - Applications, Dr. Boris Escalante (Ed.), ISBN: 978-953-51-0651-7, InTech, Available from: http://www.intechopen.com/books/remote-sensing-applications/mapping-soil-salinization-of-agricultural-coastal-areas-in-southeast-spain

INTECH
open science | open minds

InTech Europe
University Campus STeP Ri
Slavka Krautzeka 83/A
51000 Rijeka, Croatia
Phone: +385 (51) 770 447
Fax: +385 (51) 686 166
www.intechopen.com

InTech China
Unit 405, Office Block, Hotel Equatorial Shanghai
No.65, Yan An Road (West), Shanghai, 200040, China
中国上海市延安西路65号上海国际贵都大饭店办公楼405单元
Phone: +86-21-62489820
Fax: +86-21-62489821

IntechOpen